Sopu, D.; Soyarslan, C.; Sarac, B.; Bargmann, S.; Stoica, M.; Eckert, J.:
Structure-property relationships in nanoporous metallic glasses
In: Acta Materialia (2016) Elsevier

DOI: 10.1016/j.actamat.2015.12.026

Structure-property relationships in nanoporous metallic glasses

D. Şopu[a,*], C. Soyarslan[b], B. Sarac[a], S. Bargmann[b,c], M. Stoica[a,d] and J. Eckert[e,f]

[a] *IFW Dresden, Institut für Komplexe Materialien, Helmholtzstr. 20, D-01069 Dresden, Germany*
[b] *Institute of Continuum and Material Mechanics, Hamburg University of Technology, Eissendorfer Str. 42, 21073 Hamburg, Germany*
[c] *Institute of Materials Research, Helmholtz-Zentrum Geesthacht, Max-Planck Str. 1, 21502 Geesthacht, Germany*
[d] *Politehnica University of Timisoara, P-ta Victoriei 2, RO-300006 Timisoara, Romania*
[e] *Erick Schmid Institute of Materials Science, Austrian Academy of Sciences, Jahnstrasse 12, A-8700 Leoben, Austria*
[f] *Department Materials Physics, Mountanuniversität Leoben, Jahnstrasse 12, A-8700 Leoben, Austria*

Abstract

We investigate the influence of various critical structural aspects such as pore density, distribution, size and number on the deformation behavior of nanoporous $Cu_{64}Zr_{36}$ glass. By using molecular dynamics and finite element simulations an effective strategy to control the strain localization in nanoporous heterostructures is provided. Depending on the pore distribution in the heterostructure, upon tensile loading the nanoporous glass showed a clear transition from a catastrophic fracture to localized deformation in one dominant shear band, and ultimately to homogeneous plastic flow mediated by a pattern of multiple shear bands. The change in the fracture mechanism from a shear band slip to necking-like homogeneous flow is quantitative interpreted by calculating the critical shear band length. Finally, we identify the most effective heterostructure with enhanced ductility as compared to the monolithic bulk metallic glass. The heterostructure with a fraction of pores of about 3% distributed in such a way that the pores do not align along the maximum shear stress direction

*Corresponding author.
Email address: d.sopu@ifw-dresden.de (D. Şopu[a,*])

shows higher plasticity while retaining almost the same strength as the monolithic glass. Our results provide clear evidence that the mechanical properties of nanoporous glassy materials can be tailored by carefully controlling the design parameters.

Keywords: Bulk metallic glass; Nanopores; Ductility; Molecular dynamics; Finite element analysis.

---

1. Introduction

Despite the great potential of bulk metallic glasses (BMG) to be used as structural materials the inverse strength-ductility-functionality problem significantly limits the application of these materials. Different strategies to improve the ductility of BMG have been proposed in the last decades such as synthesizing composite materials reinforced with a secondary crystalline phase [1, 2, 3, 4, 5, 6], pre-deformation, such as cold rolling, [7, 8, 9], producing nanoglasses with soft glass-glass interfaces [10, 11, 12], or fabrication of porous metallic glasses [13, 14, 15, 16, 17]. In general, the role of the soft heterogeneities such as crystallites, pre-induced shear bands (SBs), interfaces or pores is to introduce strain concentrations which act as initiation sites for SBs resulting in the formation of a highly organized pattern of multiple SB formation. The extrinsic stress concentrators distributed uniformly throughout the BMG stabilizing the glass against catastrophic failure along a critical SB.

Due to the light weight, enhanced ductility and excellent electrical/thermal conductivity porous BMG can be good candidates for structural and functional applications [18]. Porous BMG with an average pore size ranging from just couple of tens of nanometers to hundreds of micrometers have been fabricated using a number of approaches [13, 14, 15, 16, 17]. However, all these techniques to fabricate such porous BMG do not allow controlled variation of structural features, such as pore spacing, size, shape, and volume fraction. Recently, a new experimental method has been proposed by Sarac and Schroers [19] to fabricate heterostructures like foams allowing a systematic variation of the structural fea-

tures. Computational investigations prove useful at this stage. The studies of [20] on the microanatomy arrangement of the porous BMG reveal that the size and configuration of the pores together with the amount of porosity can systematically control the SB propagation. When decreasing the characteristic length scale of the pores to the nanometer regime molecular dynamics (MD) simulations have revealed that the size of the pores greatly influences the initiation and propagation of SBs in BMG upon uniaxial compression [21]. In these simulations, however, free surface boundary conditions were present that promote the activation of shear transformation zones (STZ) [22]. Thus, the free surface and the pores are competing heterogeneities, and the results do not provide a clear picture of the deformation mechanism of a bulk nanoporous structure. Moreover, many critical aspects such as how the pore spacing, distribution, size, and volume fraction affect the plasticity of nanoporous BMG are not yet studied.

In this work we provide a systematic investigation on the mechanical properties of $Cu_{64}Zr_{36}$ nanoporous BMG by means of two different approaches using atomistic and continuum modeling: MD and finite element (FE) simulations, respectively. First, we investigate the size effects on the deformation mechanism by comparing our results to those obtained for heterostructures with the pore sizes in the micrometer regime [19, 20]. Then, the impact of the pore distribution on the deformation mechanism of nanoporous BMG is investigated. In addition, the optimization of strength and ductility in nanoporous BMG is discussed in terms of pore size and number. Finally, the pore architecture is tailored and the most effective heterostructure is designed which shows a high plasticity together with a yield strength quite close to the value of the monolithic BMG.

2. Simulation Approach

2.1. Molecular dynamics simulations

For studying mechanical properties of nanoporous BMG, classical MD simulations were performed using the program package LAMMPS [23]. The inter-

atomic interaction is described by the modified Finnis-Sinclair type potential for Cu-Zr binary alloys proposed by Mendelev et al. [24]. For a system with N atoms, the total energy U consists of a pairwise term and a many-body term

$$U = \sum_{i=1}^{N-1} \sum_{j=i+1}^{N} \varphi_{t_i t_j}(r_{ij}) + \sum_{i=1}^{N} \Phi_{t_j}(\rho_i), \tag{1}$$

where $t_i(t_j)$ is the element type of atom $i(j)$, φ is the pairwise potential between atom i and j separated by a distance r_{ij}, Φ is the embedded energy functional and ρ the electronic density. This potential reproduces experimental x-ray diffraction data on amorphous Cu-Zr alloys [24].

For all simulations, a constant integration time step of 2 fs was used. In the first step, a metallic glass block containing 8000 atoms was produced by quenching from the melt. After relaxation at 2000 K for 2 ns to ensure chemical homogeneity, the melt was quenched to 50 K using a cooling rate cooling rate of 0.01 K/ps. The atomic structure of the synthesized $Cu_{64}Zr_{36}$ glass shows good agreement with what has been reported in literature [25]. Next, plates of different dimensions were constructed by replicating the initial BMG block to construct a structure consisting of more than six million atoms. Nanoporous BMGs with different number of pores and distribution were created by extruding circles of diameters varying from 1.3 nm up to 18 nm in the $xz-$plane. The structures were relaxed to zero pressure at 50 K for 100 ps prior to deformation. Periodic boundary conditions were applied in all three dimensions and, hence, the pores are actually cylinders of infinite lengths.

In order to study the deformation mechanism of nanoporous BMG in comparison to the monolithic BMG the structures were deformed under uniaxial tension parallel to the $z-$direction. All structures were deformed by applying a constant strain rate of 4×10^7 1/s at a constant temperature of 50 K. The pressure in $x-$ and $y-$direction was kept zero, allowing for lateral contraction. The atomic scale deformation mechanisms were analyzed by visualizing the local atomic shear strain [26], calculated with the OVITO analysis and visualization

software [27].

2.2. Finite element analysis

The effects of pore density, size, and stacking were investigated by the finite element simulations to reinforce the argument postulated by the atomistic simulations. Albeit their unique properties originating from the amorphous structure, metallic glasses were started to be investigated through finite element methods only in the last couple of decades [28, 29, 30]. A local version of the constitutive model introduced by Bargmann et al. [31] was adopted, which is thermodynamically consistent and rate dependent [32]. For model details and its nonlocal extension the reader is referred to [31]. The model was implemented as a user defined material subroutine for ABAQUS. The used model parameters at room temperature are presented in Table 1.

Table 1: Material parameters selected for the mathematical model, [20].

Parameter	Symbol	Value	[Unit]
Young's modulus	E	86.9	[GPa]
Poisson's ratio	ν	0.37	[−]
Free volume generation factor	s_γ	0.02	[−]
Resistance to free volume	a_{res}	320	[GJm^{-3}]
Defect free energy coefficient	a_{def}	3500	[GJm^{-3}]
Strain rate sensitivity	n	50	[−]
Fully annealed free volume	ξ_0	0.09	[%]
Initial cohesion	c_0	750	[MPa]
Material strain rate	$\dot{\gamma}_0$	0.001	[s^{-1}]
Characteristic frequency	f_0	327	[s^{-1}]
Fitting constant 1	b	−300	[−]
Fitting constant 2	ϕ	0.2	[−]

The overall size of the samples, as well as the porosity and pore distribution were taken the same as in the case of atomic simulations to establish a one-to-one comparison. In the simulations explicit dynamic formulation is used.

In line with the MD simulations, periodic boundary conditions were pursued along the edges of the representative volume element (RVE). We assume plane strain conditions at a loading rate of 10^{-4} 1/s. Unlike the work of Ruan et al. [33], where loss of ellipticity instability analyses were successfully used to determine the SB initiation orientation in metallic glasses, the observed initial structures are not homogeneous and involves voids. Selection of such RVEs help to investigate the long range interaction between voids which is not captured by the unit cell models based on the average void spacing and the macroscopic stress state where lower local strains are predicted [34]. Noting that free volume is already a measure of nano-voids in metallic glass, our modeling approach stands for a bimodal pore size distribution where the apparent hole arrangements in the RVE stand for the larger void cluster. Since the constitutive theory is a local one, the results obtained does not account for size-effects. Basically, the presented results are self-similar and scale invariant as far as the identical discretization applies.

3. From micro- to nano-scale

In the first part of this work we analyze the deformation mechanisms of nanoporous BMG in comparison to the case of heterostructures with pores sizes in the micrometer regime [19, 20]. In case of microporous BMG it has been shown that by designing the pore architecture within the structure, the deformation mechanism was tuned in a systematic way, allowing to quantify the influence of each microfeatural aspect on the mechanical properties. [19, 20]. Based on these results, the improved tensile ductility originates from the formation of multiple SBs between adjacent pores within a sequence of rows. Moreover, the fracture of the heterostructure propagates perpendicular to the loading direction.

In line with these results, it is interesting to see how the deformation mechanisms change when decreasing the characteristic length scale of the pores to the nanometer regime. Thus, we constructed three nanoporous BMGs with 8

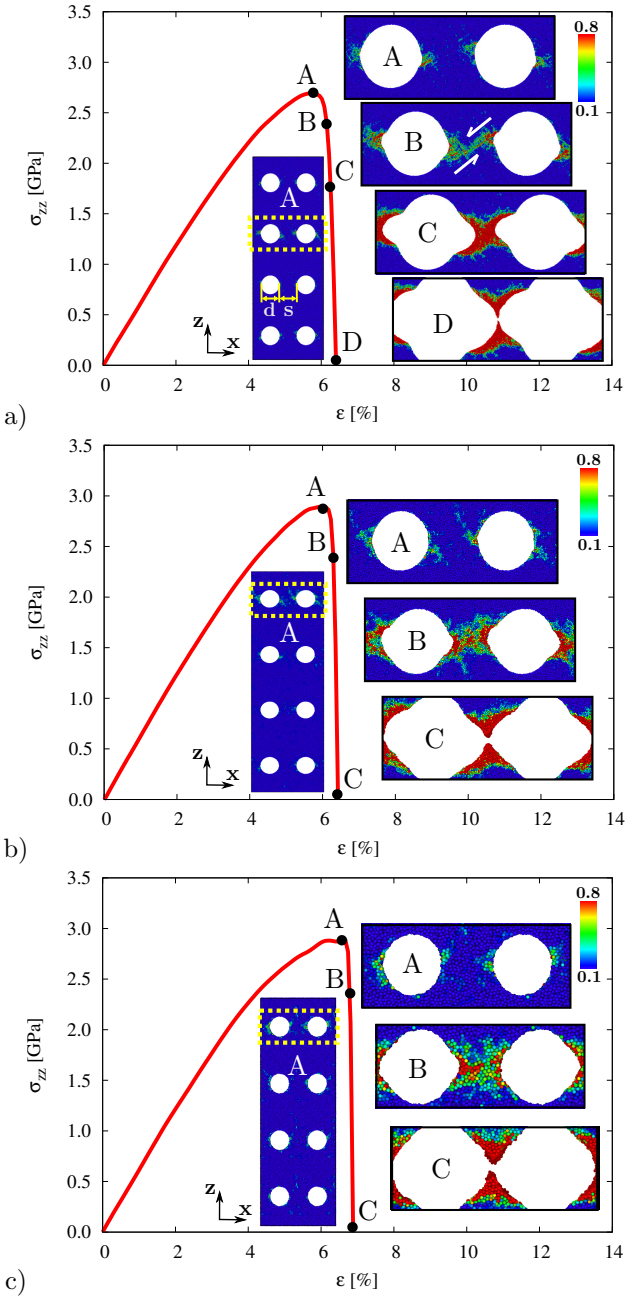

Figure 1: MD simulations: Tensile stress-strain curves together with snapshots of the local atomic shear strain along the deformation of three nanoporous BMGs with pore sizes of 18 (a), 9 (b) and 4.5 nm (c), respectively. For a better visualization of the deformation mechanism only the line of pores along which the structures deform is shown (regions with yellow boundaries).

pores and pore diameters (d) of 18, 9 and 4.5 nm, respectively. The constant spacing between the pores in lateral direction (s) is equal to the pore diameters resulting in a ratio d/s=1 (see Fig. 1(a)). For the case of heterostrustures with pore sizes in the micrometer regime, it has been shown that this ratio provides the best mechanical properties such as extensive plasticity and high yield strength [19, 20]. To preserve a constant porous-to-bulk material ratio, plates with dimensions of $18 \times 7.5 \times 50$, $36 \times 7.5 \times 112$ and $72 \times 7.5 \times 212$ nm^3, and a total number of 330987, 1525827, and 6303849 atoms, were constructed by replicating the initial BMG block.

In order to investigate the mechanical properties of these nanoporous BMGs the stress-strain curves together with snapshots of the local atomic shear strain evolution during the deformation are presented in Fig. 1. In line with the experimental work [19], we find that all three heterogeneouos structures fracture perpendicular to the loading direction (Fig. 1). However, comparing the case of the heterostructure with a pore size of 18 nm and the other two structures with smaller pores, it can be easily observed that the deformation mechanisms differ. The nanoporous BMG with a pore diameter of 18 nm exhibits a two step deformation mode: localized yielding confined in SBs followed by necking like homogeneous flow. Initially, notches are formed at the surface of the pores at a strain of about 6% marked with point A on the stress-strain curve in Fig. 1(a). These notches represent the nucleation zones for the SBs. When the plastic deformation zone size reaches the critical size compared to the SB width, SB nucleation takes place [35, 36]. The SBs are subsequently redirected towards the neighboring pore (point B) drastically lowering the applied stress. The snapshot B in Fig. 1(a) shows the formation of one mature SB between two adjacent pores. Upon loading the threshold stress level is reached, causing other small embryonic SBs to nucleate and propagate along the same line of pores. Between points B and C the SBs intersect and overlap forming a broad region with an enhanced atomic strain. From this point until the final strain level when fracture occurs (point D) the structures deform homogeneously by necking. On the other hand, when decreasing the size of the pores below 18 nm

we find a strong difference in the strain localization. For the cases of nanoporous BMGs with pore sizes of 4.5 nm and 9 nm no SBs nucleate during deformation. Thus, the yielding mechanism changes from shear slip via formation of SBs to formation of a broad necking region between the adjacent pores (see Fig. 1, panels (b) and (c)). Once the yield stress is overcome, the nanoporous BMGs deform very fast by necking and finally fracture perpendicular to the loading direction. Decreasing the size of the pores accelerate the necking process and fracture occurs faster. In Fig. 1 the stress-strain curve reveals a steeper drop of the stress to zero pressure when the size of the pore is decreased.

A quantitative interpretation of the plastic behavior of amorphous $Ni_{50}Nb_{50}$ nanowires deformed in tension proposed by Shi [37], explains that an amorphous nanowire exhibits shear banding as long as its length is bigger than the SB thickness. When the size of the nanowire drops below this value, then the structure exhibits necking instead of shear slip. Similar approaches can be applied to explain the transition in the plastic behavior of nanoporous BMGs with decreasing the pores size/interspacing. Here, the surface of the pores act like heterogeneities that promote the activation of shear transformation zones, and, therefore, trigger the formation of critical SBs. Based on Shi's formulation, the threshold pore interspacing should follow the condition that the elastic energy release is larger than the SB energy [37]. From this condition results a threshold interspacing: $l_{min} = [En\Delta w/(\sigma_Y^2 - \sigma_F^2)](2/\cos\theta)t$, where E is the Young's modulus, n is the number density, Δw is the difference between the potential energy of the SB and the undeformed bulk glass, σ_Y and σ_F are the yield and flow stress, θ is the angle between shear plane normal and the loading direction and t is half of the SB thickness. Typical parameters calculated in simulations for $Cu_{64}Zr_{36}$ BMG are t=2.5 nm, n=6.2x10^{28} m^{-3}, E=83 GPa, Δw=0.07 eV/atom, σ_Y=4.8 GPa, σ_F= 1.8 GPa and θ=40°. From here a threshold pore interspacing of about 20 nm is estimated. This estimation is crude and neglects the heat generation from elastic energy release and the possibility of partial SB formation. However, this data validates our MD results for the case of the nanoporous BMG with a pore interspacing of 18 nm, which is slightly smaller than l_{min}, where a

dominant SB forms and propagates between adjacent pores. Nevertheless, for the cases of heterostructures with pore interspacings of 9 and 4.5 nm, which are much smaller than the critical interspacing, no SB nucleate and, thus, the nanoporous BMGs deform homogeneously by necking. Therefore, in a rudimentary estimation, we expect that by further increasing the pore size in proportion to the pore spacing the plastic deformation will be carried by a higher number of SBs formed between the adjacent pores, resembling in this way the plastic behavior observed experimentally in heterostructures with micropores [19].

4. Pore distribution effects

Valuable insights about the interplay of critical microstructural aspects such as pore distribution and mechanical properties of porous BMG heterostructures have been recently provided [19, 20, 38]. The next question we address is whether in the nanometer regime the pore distribution also affects the plasticity of nanoporous BMG. For this, the case of the heterostructure with a pore size of 4.5 nm was chosen. Three nanoporous BMGs with 16 pores but with different spatial distribution were constructed. In Fig. 2, the local atomic shear strain at a strain level of 11% is presented for three heterostructures, one with an AA pore stacking and a ratio d/s=1 (left hand side panel), second with an AB pore stacking and d/s=1/2 (the middle panel) and finally, a structure with an AA stacking and d/s=1/2 (right hand side panel). It can be easily observed that each of these nanoporous BMGs shows completely different deformation behavior. Depending on the pore distribution in the nanoporous BMG, upon tensile loading the heterostructures show a clear transition from a fracture-like deformation mode perpendicular to the loading direction to localized deformation in one dominant SB, and finally to homogeneous plastic flow mediated by a pattern of multiple SBs, as can be seen in Fig. 2(a).

In order to understand this drastic transition in the deformation mechanism of the nanoporous BMGs when modifying the pore distribution, a detailed analysis of the atomic structure of these heterostructures was conducted. Character-

istic areas in each heterostructure were selected (regions with yellow boundaries in Fig. Fig. 2(a)) at two different strain levels before and after reaching the ultimate tensile strength and only those atoms with an atomic strain higher than 10% are plotted (Fig. 2(b)). In case of the nanoporous BMG with AA pore stacking and d/s=1, the material fails by fracturing perpendicular to the loading direction showing necking-like homogeneous flow. The Fig. 2(b) left hand side panel reveals that the strain fields around the neighboring pores overlap (the ellipse with black boundaries). Initially, the STZs nucleate around the pores forming notches. These notches overlap providing a continuous zone characterized by a high degree of disorder and enhanced free volume. Consequently, the heterostructure deforms via fast necking along one of these soft regions and finally fracture sets in. The fracture leads to full stress relaxation, as revealed by the stress-strain curves (blue dashed lines) plotted in Fig. 2(b). Moreover, the fracturing gives the opportunity to differentiate between elastic and plastic strain. During fracture the macroscopic stress is fully relaxed and, consequently, the elastic atomic strain around the undeformed pores is reduced leaving behind just the residual plastic strain, as can be easily seen in Fig.2(b).

When modifying the pore distribution and constructing a nanoporous BMG with an AB pore stacking and ratio d/s=1/2 the deformation mechanism changes dramatically. Now, the plastic deformation is localized in one dominant SB connecting those pores distributed in a plane inclined at about 45° with respect to the loading axis (Fig. 2, middle panels). In this case, STZs nucleate around the pores and proliferate forming a network of embryonic SBs connecting the adjacent pores. Since the pores are arranged diagonally periodic along the maximum shear stress direction, the elastic energy release during plastic deformation is sufficiently large to provide the excessive energy associated with the formation of a dominant SB by connecting the aligned embryonic SBs. The propagation of one single SB leads to a significant stress drop, as can be seen in Fig. 2(c). However, after reaching this strain level the nanoprous BMG shows a slight increase in flow stress, which is due to the fact that shear bands have to rotate in the three-dimensional periodic setup and the Schmid factor is decreasing. A similar

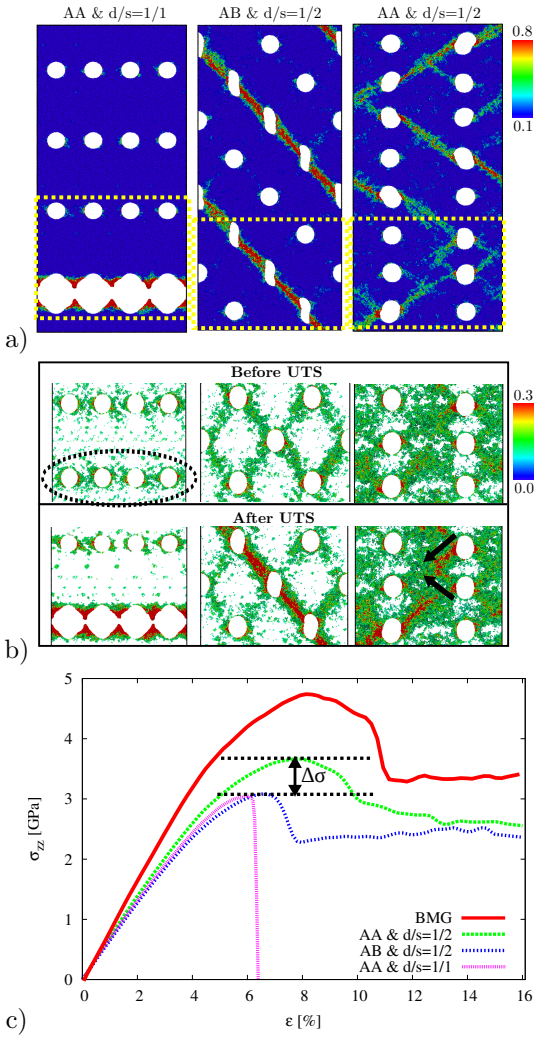

Figure 2: a) Local atomic shear strain for the case of nanoporous BMG with 16 pores of 4.5 nm and different distributions. b) For a better understanding of the plastic behavior, characteristic areas in the heterostructures are chosen and only those atoms with a local atomic strain higher than 0.1 are plotted before and after reaching the ultimate tensile strength (UTS). The ellipse with black boundaries shows that the strain fields overlap given that the pore interdistance is smaller than the pore diameter. c) Tensile stress-strain curves for these nanoporous BMGs at a strain rate of $4{\cdot}10^7 s^{-1}$.

effect is found in all structures which show localized deformation in one dominant SB such as the monolithic BMG (see Fig. 2(c)). We should also mention that during post data processing the structure dimensions are affine transform so that the shape of the structures will not change during tensile load. Hence, the shear band angle will not deviate from the initial value during deformation.

The third nanoporous BMG investigated here, with an AA pore stacking and d/s=1/2, has revealed the best plastic behavior. This structure shows homogeneous plastic flow, mediated by a network of multiple SBs, together with an increased maximum stress. In order to explain the improved plasticity, we also analyzed the local atomic shear strain. Fig. 2(a), right hand side panels, reveals that embryonic SBs nucleate at the pore surfaces and propagate to the next pore along an angle of about 60° with respect to the loading axis. The angle deviation from the maximum shear stress direction results in the formation of SBs with high energy. Therefore, the elastic energy release during plastic deformation is not enough to provide the excessive energy associated with the formation of a dominant SB. In return, many embryonic SBs form and none of those goes critical. Moreover, the embryonic SBs intersect and block each other before touching the next pore (as marked with arrows in Fig. 2(b)), manifesting a strain hardening process. Fig. 2(c) reveals an increase in the maximum stress equivalent to $\Delta\sigma$=0.5 GPa. Therefore, the maximum stress at which these embryonic SBs propagate to the next pore is higher compared to the other two nanoporous BMGs. Furthermore, due to the intersection of SBs, the released elastic energy is used to nucleate a higher fraction of STZs in the heterostructure, as can be seen in Fig. 2(b)).

5. Strength-ductility optimization

The goal of this work is to identify the most effective nanoporous BMG structure in terms of high plasticity and high yield strength. As shown in the previous section, the heterostructure with 16 pores with a diameter of 4.5 nm distributed with an AA stacking and d/s=1/2 has shown the best plastic be-

havior. Nevertheless, since pores are soft heterogeneities, a high fraction of porosity results in a drastic decrease of the heterostructures strength. From the stress-strain curve plotted in Fig. 2(c) maximum stress of about 3.7 GPa is found which is much lower in comparison to the value of the monolithic BMG with the same chemical composition (σ_{max} ≈4.8 GPa). Therefore, the next questions we address is whether the maximum stress of nanoporous BMG can be increased while avoiding localized plastic deformation by decreasing the number or/and size of the pores. First, the impact of the pore density on the plastic mechanisms is investigated by decreasing the number of the soft heterogeneities from 16 to 8. When analyzing comparatively the plastic behavior of these two heterostructures with pores distributed in an AA stacking with d/s=1/2, a completely different deformation mechanism has been found. With decreasing number of pores the deformation switches from homogeneous plastic flow mediated by a pattern of multiple SBs to a localized deformation in one dominant SB (see Fig. 3). Moreover, due to the localized plastic deformation the maximum stress does not increase significantly by decreasing the number of pores. The stress-strain curves of the two structures plotted in Fig. 3 reveal a small difference between the two maxima. Nevertheless, the stress-strain curve of the heterostructure with 8 pores shows a stress drop when shear band sets in, in contrast to the curve for the heterostructure with 16 pores where a smooth stress relaxation occurs. Calculating the angle formed between the SB and the loading axis we found a value of about 45° (see Fig. 3). Therefore, the spatial distribution of the pores in the structure allows the SB to propagate along the maximum shear stress direction to go critical and form a dominant one. In order to avoid the formation of a dominant SB we constructed a new heterostruture in which the pores were distributed in such a way that the embryonic SBs formed between the adjacent pores had an angle of about 60° with respect to the loading axis. Fig. 3 reveals that the new heterostructure shows homogeneous plastic flow mediated by a network of multiple SBs similar to the case of the heterostructure with 16 pores. This statement is corroborated by the stress-strain curve which shows a smooth stress relaxation.

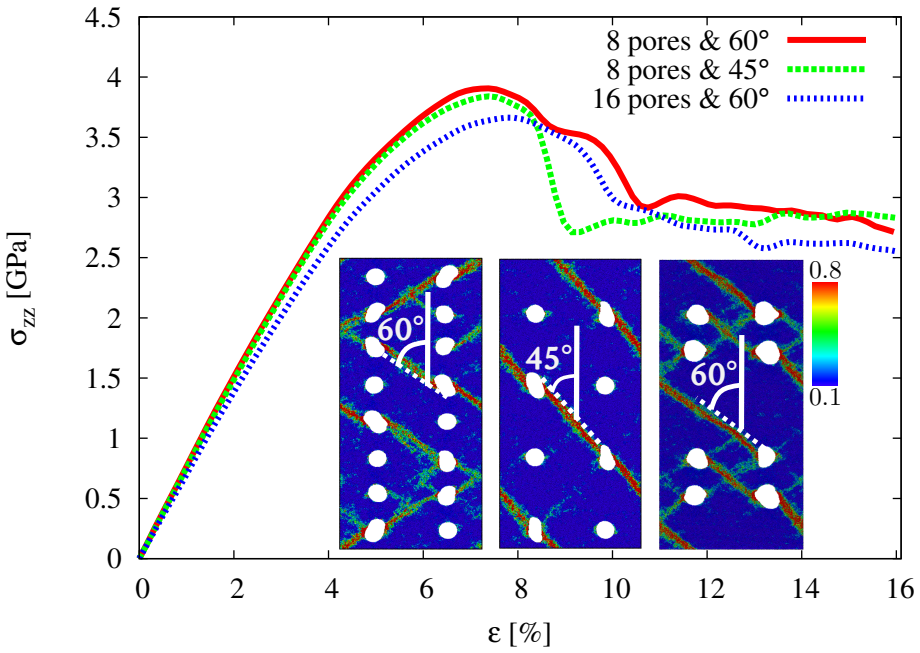

Figure 3: Tensile stress-strain curves for nanoporous BMGs with 16 and 8 pores and different distribution, repectively, and a diameter of 4.5 nm at a strain rate of $4{\cdot}10^7 s^{-1}$. Three snapshots with the local atomic shear strain of these heterostructure at a strain level of 16% are also presented.

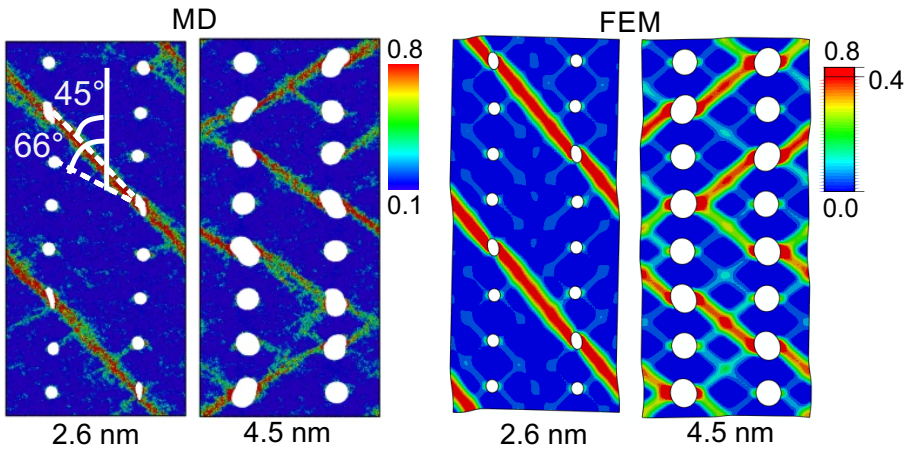

Figure 4: Local atomic shear strain from MD simulations and equivalent plastic strain distributions from FE simulations of the heterostructure with pores of 2.6 nm and 4.5 nm. Both methods reveal similar plastic behavior under tensile deformation.

The next approach to increase the yield strength of nanoporous BMGs while retaining their ductility is to decrease the size of the pores. Fig. 4 presents the comparative plastic behavior of two heterostructures with an AA stacking and d/s=1/2 and a pore size of 4.5 nm and 2.6 nm, respectively. When decreasing the size of the pores to 2.6 nm, the deformation mechanism turns from homogeneous plastic flow to shear band slip. However, the dominant SB forms no more between the pores of two consecutive rows, as found in the case of the heterostructure with pores of 4.5 nm and an angle of 60° in between. The decrease in the pore size results in an increase in the pore spacing in the lateral direction perpendicular to the loading axis since these parameters are not mutually exclusive, i.e. modification of one directly affects the other. Calculating the angle between two consecutive rows of pores the angle increases from 60° to 66° with decreasing pore size (see Fig. 4). The excessive energy associated with the formation of a SB increases by deviating from the plane of maximum shear stress. Hence, a mature SB forms between i and i+2 lines of pores, where i represents the index of the row. This SB goes critical along the maximum shear stress direction ($\approx$ 45°) instead of choosing the 66° angle.

A comparable study of the plastic behavior of nanoporous BMGs was conducted using also a continuum approach. By means of the finite element method we investigated the mechanical properties of the two heterostructures with the same overall size of the samples, as well as the porosity and pore size as in the case of MD simulations to establish a one-to-one comparison. Both studies show very good agreement in terms of deformation mechanism and the evolution of shear bands in the direction of the highest resolved shear stress in the course of tensile deformation. In the finite element simulations the development of shear bands is as follows: Under loading, around introduced voids stress concentrations occur at which early plastic deformation initiate. Long range interactions take place between voids, and together with the coupled nature of plastic shearing and free-volume generation, weak deformation bands emerge. These bands show a symmetric pattern which cross the boundaries of the RVE. The softening material response due to free volume generation and shear instability causes a symmetry-breaking bifurcation. Following, intense straining concentrates on one of the bands only, whereas others become less pronounced. Naturally, in the MD simulations the symmetry is broken due to the random distribution of atoms in the glassy matrix, whereas in the FEM the source is the finite precision arithmetics. In the current case long range interactions between the voids dominate and control the SB angle. In agreement with our MD simulation results, the heterostructure with smaller voids shows nearly 45° band orientation while for the system with larger voids the SB angle increases. Moreover, the band thicknesses observed in the FEM simulations are in accordance with our MD analysis. This complies well with the reported qualitative FEM-MD agreement with [30] and [39] also with the TEM studies suggesting a SB thickness of 10 nm, [40].

Fig. 4 reveals also a transition in the deformation mechanism from homogeneous plastic flow to localized deformation in a dominant SB with decreasing size of the pores. Similar to MD simulations, the most non-uniform nature of the deformation is observed for the case with regular void distributions of 2.6 nm. Therefore, this might be an indication that creating a low fraction of poros-

ity is beneficial for the mechanical properties of nanoporous BMGs given that the resulting pore architecture does not allow for aligning the pores periodically along the maximum shear stress direction.

6. Tailoring the pore architecture

The results discussed above demonstrate a strong correlation between the pore distribution, size and density, in a way where it is not feasible to modify one of these parameters without affecting the others. Therefore, we tried to design an ideal nanoporous BMG structure with enhanced ductility while holding the maximum stress closer to the value of the monolithic BMG. The construction of such a structure must follow the criteria that the pores should not be aligned along the maximum shear stress direction and their volume fraction must be high enough so that the applied strain is distributed uniformly throughout the heterostructure avoiding the formation of a critical SB.

Based on these criteria we constructed a nanoporous BMG with 16 pores of 2.6 nm diameter distributed in a honeycomb-like pattern, as can be seen in Fig. 5. Modifying the pore distribution from an AA stacking and d/s=1/2 to a honeycomb geometry we found a transition from localized deformation to homogeneous plastic flow. The formation of a pattern of multiple SBs, which intersect and block each other, results in a smoother stress relaxation compared to the case of monolithic BMG (see Fig. 6). At a strain level of 10% embryonic SBs nucleate at the pore surface and orient along a direction of 45° with respect to the loading axis, as can be seen in Fig. 5. Since they block each other, a high number of embryonic SBs is formed and distributed over the whole sample so that the local energy release is not sufficient to accelerate one of these SBs. Moreover, at a strain of 12% these embryonic SBs start to diverge from their initial direction and propagate to an adjacent pore forming a mature SB oriented along a 60° direction with respect to the load axis. Even at a strain of 15% none of these SBs goes critical and, hence, the nanoporous BMG deforms homogeneously.

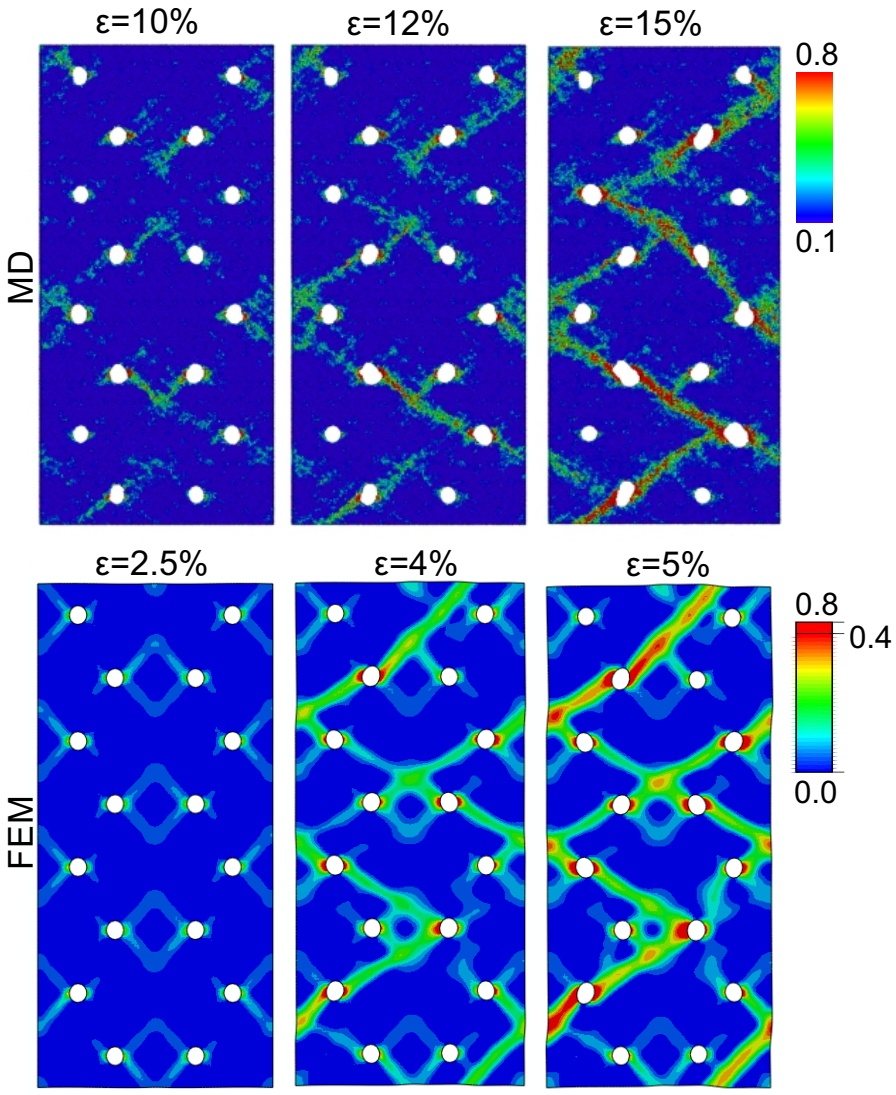

Figure 5: Local atomic shear strain and the equivalent plastic strain distributions at different strain levels under tensile deformation of the nanoporous BMG with pores of 2.6 nm and a honeycomb-like pore distribution.

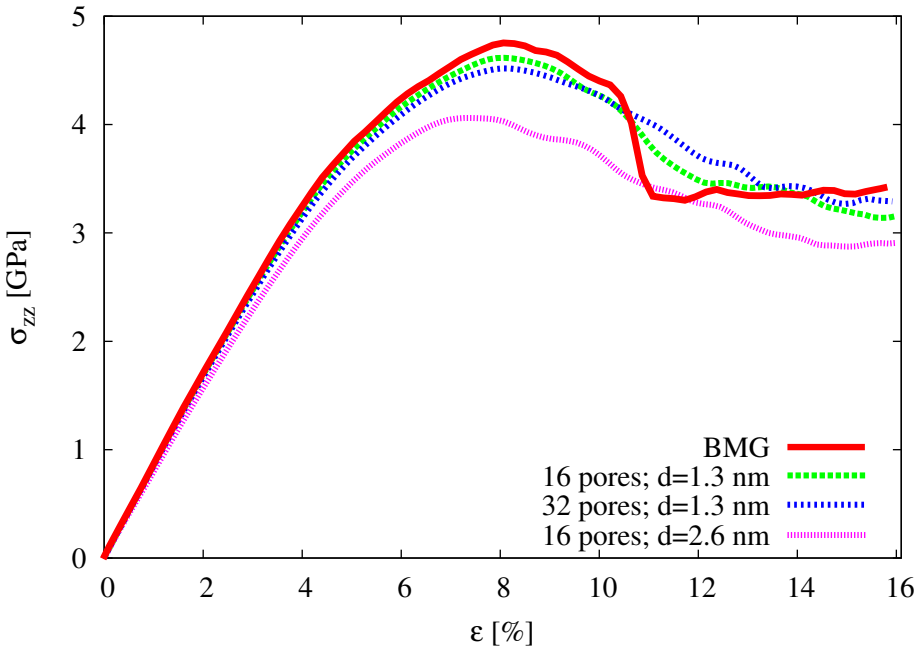

Figure 6: Tensile stress-strain curves of two nanoporous BMGs with 16 pores of 2.6 nm and 1.3 nm and one with 32 pores of 1.3 nm in comparison with a monolithic BMG at a strain rate of $4{\cdot}10^7 s^{-1}$.

Again, the finite element simulations provide an excellent qualitative agreement with MD simulations in terms of homogeneously localized strain distribution in the nanoporous BMG. However, the nominal strains in the FEM study are lower than the corresponding nominal strains of MD simulations. Aside from other possible sources, this difference mainly arises from a large difference between the strain rates of FEM and MD simulations. As simulations show, as the deformation proceeds, the pores distribution results in a proliferation of multiple shear bands, and hence, the material response becomes relatively more ductile with higher energy absorption.

In case of composite materials, shear events start at the interfaces between glass and crystalline precipitate and form SBs which cannot freely propagate throughout the sample since they are partly blocked by other precipitates [2, 41, 3, 4]. A pore is also a defect acting like a SB nucleation site, and has it been

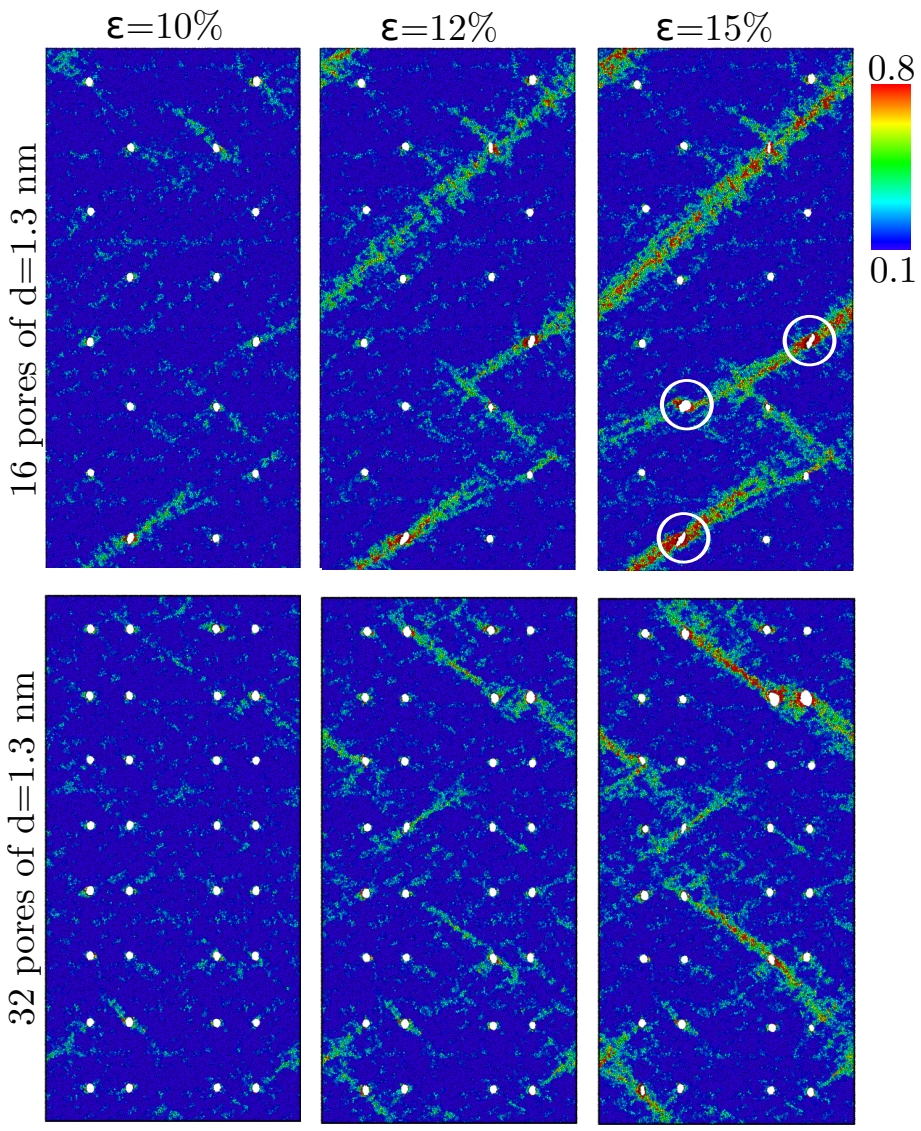

Figure 7: Local atomic shear strain at different strain level under tensile deformation of two nanoporous BMGs with 16 and 32 pores of 1.3 nm and different distribution. The white circles mark the pores which affect the SB propagation.

shown that the size of the pores greatly influences the initiation and propagation of SBs in the metallic glass [21]. However, is not clear if the size of the pore has a strong impact on the shear resistance. We have shown that the deformation mechanism of nanoporous BMGs is mostly affected by the pore distribution and density. Even for the case of a heterostructure with small pores of 2.6 nm distributed in a honeycomb-like pattern, which is less than half the width of a SB, none of the embryonic SBs can become mature into extended defects and the deformation becomes homogeneous. Therefore, we expect that nanoporous BMGs with even smaller pores show a homogeneous plastic deformation.

To test this last hypothesis, a nanoporous BMG with smaller pores of 1.3 nm was investigated. Fig. 7, upper panels, reveals a more localized deformation with decreasing size of the pores. The fraction of pores relative to the total volume of the structure is just about 1.5%. Therefore, the low fraction of pores can not distribute the applied strain homogeneously and a mature SB forms in the nanoporous BMG. Nevertheless, the impact of pores over the plastic behavior is still pronounced. Although the strain localization partially gets independent of the extrinsic stress concentrators, at least three pores, marked with circles in Fig. 7, drastically affect the SB propagation, distinguished in this way from the case of shear banding like in a defect-free sample. It has been shown for composite materials that the size of crystalline precipitates must be at least twice the SB thickness to block the propagation of a SB [5]. If the precipitates are smaller than the SB is only partially blocked or the precipitates are penetrated by the SB and undergo significant rigid motion [42]. However, in nanoporous BMGs even a very small pore of 1.3 nm partially affects the SB propagation. The dominant SB intersects with three pores altering in this way its forward propagation. The pores are not blocking the SB as found in case of composite materials. Instead, the pores act like elastic buffers for shearing. When the SB hits the pores its energy is absorbed and used to expand these pores. It can be seen in Fig 7 that the pores marked with white circles show a larger volume. The SB interaction with the pores is also revealed by the stress-strain curves plotted in Fig. 6. The stress release is much smoother in case

of nanoporous BMG compared to the monolithic BMG where a characteristic stress drop is present when shear band slip sets in. Moreover, the maximum stress of the nanoporous BMG has almost the same value as for the monolithic BMG. Therefore, in order to avoid strain localization and formation of a major SB, the pore size is not critical as long as a high extrinsic stress concentrator is involved, so that the plastic strain is homogeneously distributed over the whole sample. In order to corroborate the aforementioned statement we constructed a heterostructure with 32 pores of 1.3 nm. It can be clearly seen in Fig. 5, bottom panels, that no dominant SB formed in the heterostructure deformed at an elevated strain level of 15 %. Thus, this heterostructure with a volume fraction of pores of about 3% shows homogeneous plastic deformation while maintaining a maximum stress close to the value of the monolithic BMG. This is analogous to the literature that microporous BMGs with an overall porosity smaller than 4% showed a dramatically enhanced plasticity in compression while their Young's modulus and yield strength were slightly reduced [15].

7. Conclusions

In this paper, we have systematically investigated by means of molecular dynamics and finite element simulations the nanostructure-property relationships in $Cu_{64}Zr_{36}$ nanoporous BMG by modifying the structural architecture via pore design. Valuable insights about the interplay of critical structural aspects such as pore density, distribution, size, number and deformation mechanisms of these heterostructures have been found. In a good agreement with the experimental work on microporous BMGs, the nanoporous structures with a pore size higher than 18 nm and diameter to spacing ratio of one deform through the formation of multiple shear bands between the pores followed by a fracture-like deformation mode perpendicular to the loading direction. Furthermore, with decreasing the size of pores, we found a transition in the plastic behavior from shear banding to necking-like homogeneous flow, which has been quantitatively interpreted by calculating the critical shear band length. In addition, depending on the pore

distribution in the heterostructure, upon tensile loading the nanoporous BMG showed a clear transition from a fracture-like deformation mode to localized deformation in one dominant shear band, and ultimately to homogeneous plastic flow mediated by a pattern of multiple shear bands. Finally, most effective heterostructure with a high plasticity and yield strength closer to the value of the monolithic BMG has been identified. The construction of such a structure must satisfy the following criteria:

(i) The pores should not be periodically distributed along the maximum shear stress direction.

(ii) A high extrinsic stress concentrator (pores) must be involved to distribute the plastic strain homogeneously over the whole sample.

(iii) The size of the pores can be decreased to only 1 nm as long as an overall porosity higher than 3% is created in the heterostructure.

The results indicate that the mechanical properties of nanoporous BMG can be tailored by carefully choosing the density, fraction and spatial distribution of pores. This study can also shed a light on the investigation of the structure-property relationship of other complex BMG composites reinforced with a systematic secondary phase design on the nano-level.

8. Acknowledgment

The authors acknowledge financial support of the European Research Council under the ERC Advanced Grant INTELHYB (grant ERC-2013-ADG-340025) and the German Science Foundation (DFG) under the Leibniz Program (grant EC 111/26-1). A DAAD-PPP travel grant is also acknowledged. The authors gratefully acknowledge the computing time granted by the John von Neumann Institute for Computing (NIC) and provided on the supercomputer JUROPA at the Jülich Supercomputing Centre (JSC). Additional computing time was made available by the Center for Information Services and High Performance Computing (ZIH) at TU Dresden. The authors also thank Ulrike Nitzsche for technical assistance concerning the computer simulations.

References

[1] G. He, J. Eckert, W. Löser, L. Schultz, Novel Ti-base nanostructure-dendrite composite with enhanced plasticity, Nat. Mater. 2 (1) (2003) 33–7.

[2] C. Fan, A. Inoue, Improvement of mechanical properties by precipitation of nanoscale compound particles in Zr-Cu-Pd-Al amorphous alloys, Mater. Trans., JIM 38 (12) (1997) 1040–1046.

[3] C. C. Hays, C. P. Kim, W. L. Johnson, Microstructure controlled shear band pattern formation and enhanced plasticity of bulk metallic glasses containing in situ formed ductile phase dendrite dispersions, Phys. Rev. Lett. 84 (13) (2000) 2901–2904.

[4] C. C. Hays, C. P. Kim, W. L. Johnson, Improved mechanical behavior of bulk metallic glasses containing in situ formed ductile phase dendrite dispersions, Mater. Sci. Eng., A 304 (2001) 650–655.

[5] J. Eckert, J. Das, S. Pauly, C. Duhamel, Mechanical properties of bulk metallic glasses and composites, Journal of Materials Research 22 (2007) 285–301. doi:10.1557/jmr.2007.0050.
URL http://journals.cambridge.org/article_S0884291400092554

[6] S. Pauly, S. Gorantla, G. Wang, U. Kühn, J. Eckert, Transformation-mediated ductility in CuZr-based bulk metallic glasses, Nat. Mater. 9 (6) (2010) 473–477.

[7] M. H. Lee, K. S. Lee, J. Das, J. Thomas, U. Kühn, J. Eckert, Improved plasticity of bulk metallic glasses upon cold rolling, Scripta Mater. 62 (9) (2010) 678–681.

[8] S. Scudino, K. B. Surreddi, J. Eckert, Mechanical properties of cold-rolled Zr60Ti5Ag5Cu12.5Ni10Al7.5 metallic glass, Phys. Status Solidi A 207 (5) (2010) 1118–1121.

[9] Q. P. Cao, J. W. Liu, K. J. Yang, F. Xu, Z. Q. Yao, A. Minkow, H. J. Fecht, J. Ivanisenko, L. Y. Chen, X. D. Wang, S. X. Qu, J. Z. Jiang, Effect of pre-existing shear bands on the tensile mechanical properties of a bulk metallic glass, Acta Mater. 58 (4) (2010) 1276–1292.

[10] J. Jing, A. Kramer, R. Birringer, H. Gleiter, U. Gonser, Modified atomic structure in a Pd-Fe-Si nanoglass : A Mössbauer study, J. Non-Cryst. Solids 113 (2-3) (1989) 167–170.
URL http://www.sciencedirect.com/science/article/B6TXM-48CXMM7-V3/2/0f05e9baad09654aa30abff391ba440a

[11] D. Şopu, K. Albe, Y. Ritter, H. Gleiter, From nanoglasses to bulk massive glasses, Appl. Phys. Lett. 94 (19) (2009) 191911– 191914. doi:http://dx.doi.org/10.1063/1.3130209.
URL http://scitation.aip.org/content/aip/journal/apl/94/19/10.1063/1.3130209

[12] D. Şopu, Y. Ritter, H. Gleiter, K. Albe, Deformation behavior of bulk and nanostructured metallic glasses studied via molecular dynamics simulations, Phys. Rev. B 83 (10) (2011) 100202. doi:10.1103/PhysRevB.83.100202.

[13] A. Brothers, D. Dunand, Amorphous metal foams , Scripta Mater. 54 (4) (2006) 513 – 520, viewpoint set no. 38 on: Frontiers on fabrication and properties of porous and cellular metallic materials. doi:http://dx.doi.org/10.1016/j.scriptamat.2005.10.048.
URL http://www.sciencedirect.com/science/article/pii/S1359646205006871

[14] J. Jayaraj, J. Park, P. Gostin, E. Fleury, A. Gebert, L. Schultz, Nano-porous surface states of TiYAlCo phase separated metallic glass, Intermetallics 17 (12) (2009) 1120 – 1123. doi:http://dx.doi.org/10.1016/j.intermet.2009.05.008.

URL http://www.sciencedirect.com/science/article/pii/S0966979509001411

[15] T. Wada, A. Inoue, A. L. Greer, Enhancement of room-temperature plasticity in a bulk metallic glass by finely dispersed porosity, Appl. Phys. Lett. 86 (25) (2005) 251907–251910. doi:http://dx.doi.org/10.1063/1.1953884.
URL http://scitation.aip.org/content/aip/journal/apl/86/25/10.1063/1.1953884

[16] A. Inoue, T. Wada, D. V. Louzguine-Luzgin, Improved mechanical properties of bulk glassy alloys containing spherical pores , Mater. Scie. and Engin.: A 471 (12) (2007) 144 – 150. doi:http://dx.doi.org/10.1016/j.msea.2006.10.172.
URL http://www.sciencedirect.com/science/article/pii/S0921509307004571

[17] M. Myers, S. Charnvanichborikarn, C. Wei, Z. Luo, G. Xie, S. Kucheyev, D. Lucca, L. Shao, Phase transition, segregation and nanopore formation in high-energy heavy-ion-irradiated metallic glass, Scripta Mater. 67 (11) (2012) 887 – 890. doi:http://dx.doi.org/10.1016/j.scriptamat.2012.08.015.
URL http://www.sciencedirect.com/science/article/pii/S1359646212005258

[18] J. S. Yu, Y. Ding, C. X. Xu, A. Inoue, T. Sakurai, M. W. Chen, Nanoporous metals by dealloying multicomponent metallic glasses, Chem. Mater. 20 (14) (2008) 4548–4550. doi:10.1021/cm8009644.

[19] B. Sarac, J. Schroers, Designing tensile ductility in metallic glasses, Nat. Commun. 4 (2013) 1–7, 208XR Times Cited:8 Cited References Count:43. doi:Doi10.1038/Ncomms3158.
URL <GotoISI>://WOS:000323716300028

[20] B. Sarac, B. Klusemann, T. Xiao, S. Bargmann, Materials by design: An experimental and computational investigation on the microanatomy arrangement of porous metallic glasses, Acta Mater. 77 (2014) 411–422, an0vx Times Cited:0 Cited References Count:56. doi:DOI10.1016/j.actamat.2014.05.053.
URL <GotoISI>://WOS:000340303200037

[21] J. T. Wang, P. D. Hodgson, J. D. Zhang, W. Y. Yan, C. H. Yang, Effects of pores on shear bands in metallic glasses: A molecular dynamics study, Comput. Mater. Sci. 50 (1) (2010) 211–217. doi:10.1016/j.commatsci.2010.08.001.
URL <GotoISI>://WOS:000284250700029

[22] D. Şopu, K. Albe, Influence of grain size and composition, topology and excess free volume on the deformation behavior of CuZr nanoglasses, Beilstein J. Nanotechnol. 6 (2015) 537–545. doi:10.3762/bjnano.6.56.

[23] S. Plimpton, Fast Parallel Algorithms For Short-Range Molecular-Dynamics, J. Comput. Phys. 117 (1) (1995) 1–19.

[24] M. I. Mendelev, D. J. Sordelet, M. J. Kramer, Using atomistic computer simulations to analyze x-ray diffraction data from metallic glasses, J. Appl. Phys. 102 (4) (2007) 043501. doi:10.1063/1.2769157.
URL http://link.aip.org/link/?JAP/102/043501/1

[25] Y. Q. Cheng, A. J. Cao, H. W. Sheng, E. Ma, Local order influences initiation of plastic flow in metallic glass: Effects of alloy composition and sample cooling history, Acta Mater. 56 (18) (2008) 5263–5275.

[26] F. Shimizu, S. Ogata, J. Li, Theory of shear banding in metallic glasses and molecular dynamics calculations, Mater. Trans. 48 (11) (2007) 2923–2927.

[27] A. Stukowski, Visualization and analysis of atomistic simulation data with OVITO-the Open Visualization Tool, Modell. Simul. Mater. Sci. Eng. 18 (1) (2010) 015012.

[28] R. Huang, Z. Suo, J. H. Prevost, W. D. Nix, Inhomogeneous deformation in metallic glasses, J. Mech. Phys. Solids 50 (5) (2002) 1011–1027.

[29] Y. F. Gao, An implicit finite element method for simulating inhomogeneous deformation and shear bands of amorphous alloys based on the free-volume model, Modell. Simul. Mater. Sci. Eng. 14 (8) (2006) 1329–1345, 128CU Times Cited:34 Cited References Count:25. doi:Doi10.1088/0965-0393/14/8/004.
URL <GotoISI>://WOS:000243635500004

[30] P. Thamburaja, Length scale effects on the shear localization process in metallic glasses: A theoretical and computational study, J. Mech. Phys. Solids 59 (8) (2011) 1552 – 1575. doi:http://dx.doi.org/10.1016/j.jmps.2011.04.018.
URL http://www.sciencedirect.com/science/article/pii/S0022509611000883

[31] S. Bargmann, T. Xiao, B. Klusemann, Computational modelling of submicron-sized metallic glasses, Philos. Mag. 94 (1) (2014) 1–19. doi:10.1080/14786435.2013.838326.

[32] B. Svendsen, S. Bargmann, On the continuum thermodynamic rate variational formulation of models for extended crystal plasticity at large deformation, J. Mech. Phys. Solids 58 (9) (2010) 1253–1271, 652DY Times Cited:20 Cited References Count:64. doi:DOI10.1016/j.jmps.2010.06.005.
URL <GotoISI>://WOS:000281982800006

[33] H. Ruan, L. Zhang, J. Lu, A new constitutive model for shear banding instability in metallic glass , Int. J. Solids Struct. 48 (21) (2011) 3112 – 3127. doi:http://dx.doi.org/10.1016/j.ijsolstr.2011.07.004.
URL http://www.sciencedirect.com/science/article/pii/S0020768311002514

[34] R. Becker, R. Smelser, Simulation of strain localization and fracture between holes in an aluminum sheet, J. Mech. Phys. Solids 42 (5) (1994) 773 – 796. doi:http://dx.doi.org/10.1016/0022-5096(94)90042-6.
URL http://www.sciencedirect.com/science/article/pii/0022509694900426

[35] Z.-D. Sha, Q.-X. Pei, V. Sorkin, P. S. Branicio, Y.-W. Zhang, H. Gao, On the notch sensitivity of CuZr metallic glasses, Appl. Phys. Lett. 103 (8) (2013) 081903–081909. doi:http://dx.doi.org/10.1063/1.4819099.
URL http://scitation.aip.org/content/aip/journal/apl/103/8/10.1063/1.4819099

[36] Z. D. Sha, Q. X. Pei, Z. S. Liu, Y. W. Zhang, T. J. Wang, Necking and notch strengthening in metallic glass with symmetric sharp-and-deep notches, Sci. Reports 5 (2015) 10797–10802.
URL http://dx.doi.org/10.1038/srep10797

[37] Y. F. Shi, Size-independent shear band formation in amorphous nanowires made from simulated casting, Appl. Phys. Lett. 96 (12) (2010) 121909–121012, 575OQ Times Cited:20 Cited References Count:26. doi:Artn121909Doi10.1063/1.3340908.
URL <GotoISI>://WOS:000276077200021

[38] B. Sarac, J. Wilmers, S. Bargmann, Property optimization of porous metallic glasses via structural design , Mater. Lett. 134 (2014) 306 – 310. doi:http://dx.doi.org/10.1016/j.matlet.2014.07.064.
URL http://www.sciencedirect.com/science/article/pii/S0167577X14013238

[39] Y. Shi, M. L. Falk, Atomic-scale simulations of strain localization in three-dimensional model amorphous solids, Phys. Rev. B 73 (2006) 214201. doi:10.1103/PhysRevB.73.214201.
URL http://link.aps.org/doi/10.1103/PhysRevB.73.214201

[40] Y. Zhang, G. A.L., Thickness of shear bands in metallic glasses, Appl. Phys. Lett. 89 (2006) 071907.

[41] Y. Shi, M. L. Falk, A computational analysis of the deformation mechanisms of a nanocrystalmetallic glass composite, Acta Mater. 56 (5) (2008) 995 – 1000. doi:http://dx.doi.org/10.1016/j.actamat.2007.11.005.
URL http://www.sciencedirect.com/science/article/pii/S1359645407007513

[42] K. Albe, Y. Ritter, D. Şopu, Enhancing the plasticity of metallic glasses: Shear band formation, nanocomposites and nanoglasses investigated by molecular dynamics simulations, Mech. Mater. 67 (0) (2013) 94 – 103, nanostructured Materials. doi:http://dx.doi.org/10.1016/j.mechmat.2013.06.004.
URL http://www.sciencedirect.com/science/article/pii/S0167663613001117